SUPPORTING INFORMATION

Mechanistic Insights into Photocatalytic Reduction of Nitric Oxide to Nitrogen on Oxygen-Deficient Quasi-Two-Dimensional Bismuth-Based Perovskite

Reshalaiti Hailili,[a,‡] Zhi-Qiang Wang,[b,‡] Hongwei Ji,[a] Chuncheng Chen,[a] Xue-Qing Gong,[b,*] Hua Sheng,[a,*] and Jincai Zhao[a]

[a]*Key Laboratory of Photochemistry, Institute of Chemistry, Chinese Academy of Sciences, Beijing National Laboratory for Molecular Sciences, Beijing 100190, P. R. China.*

[b]*Key Laboratory for Advanced Materials and Joint International Research Laboratory for Precision Chemistry and Molecular Engineering, Feringa Nobel Prize Scientist Joint Research Center, Centre for Computational Chemistry and Research Institute of Industrial Catalysis, School of Chemistry and Molecular Engineering, East China University of Science and Technology, Shanghai 200237, P. R. China.*

[‡]*These authors contributed equally to this work.*

CONTENTS

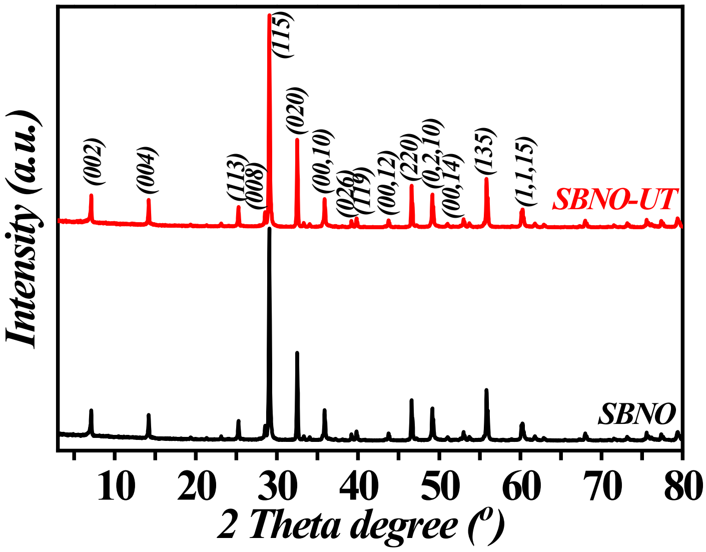

Figure SI. XRD patterns of uniform dispersed SBNO nanosheets (with 94% product yields) and ultrathin nanosheets of SBNO (SBNO–UT) (with 98% product yields).

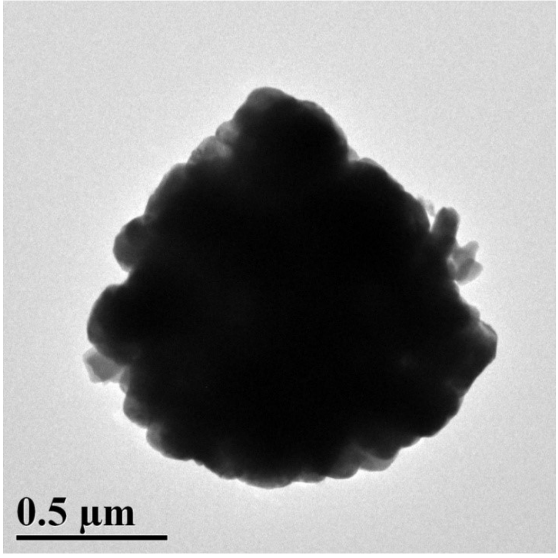

Figure S2. TEM images of SBNO.

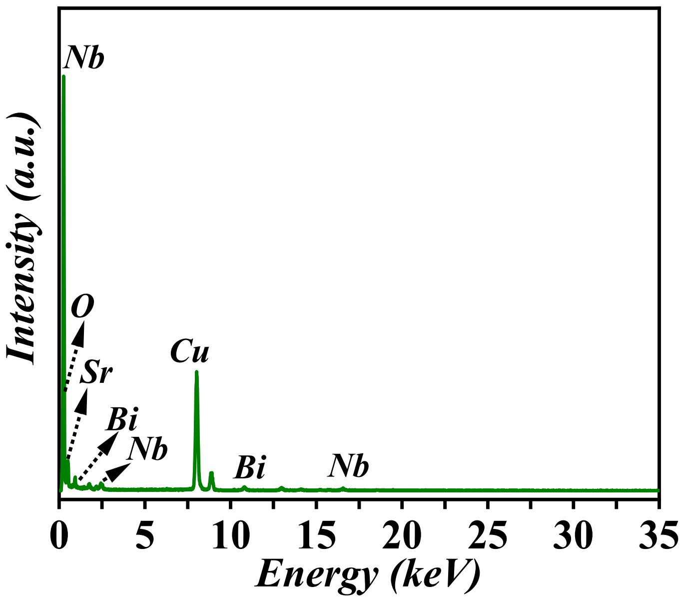

Figure S3. EDS spectra of SBNO–UT samples.

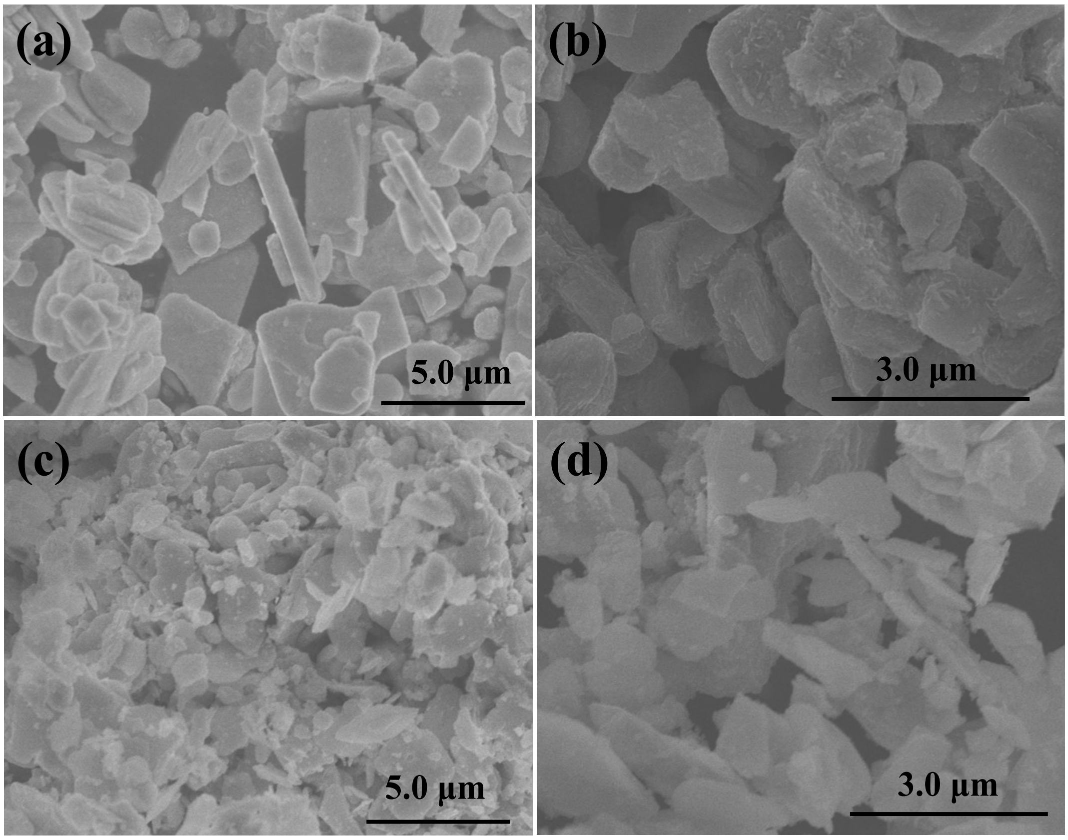

Figure S4. SEM images of SBNO samples prepared in HCl aqueous solution.

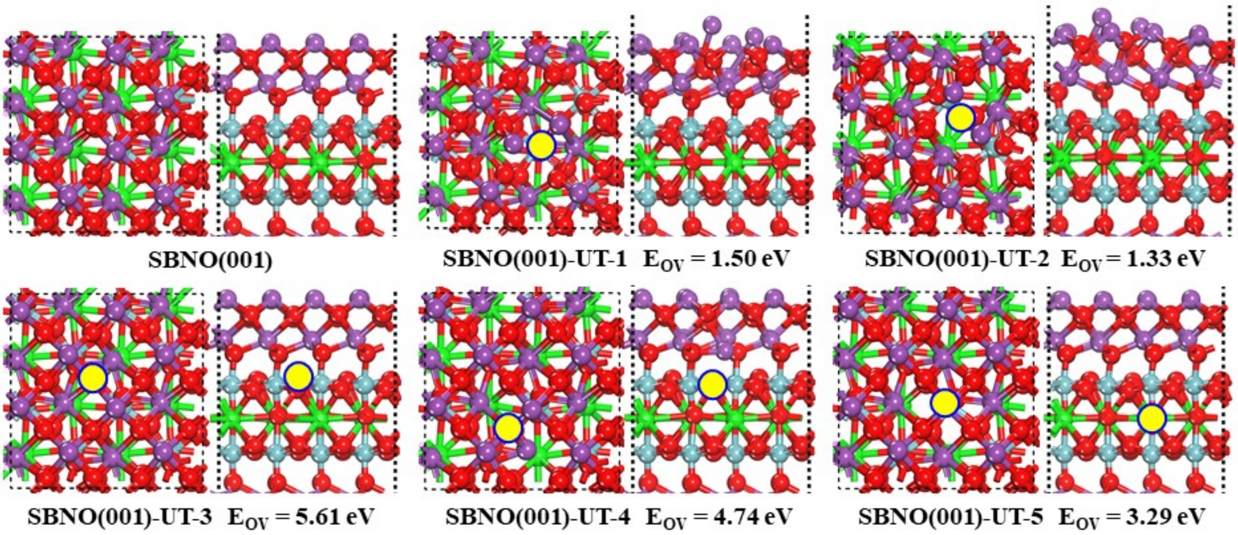

Figure S5. Calculated the structures and the vacancy formation energies of oxygen with assorted coordination environments on the SBNO (001) surface.

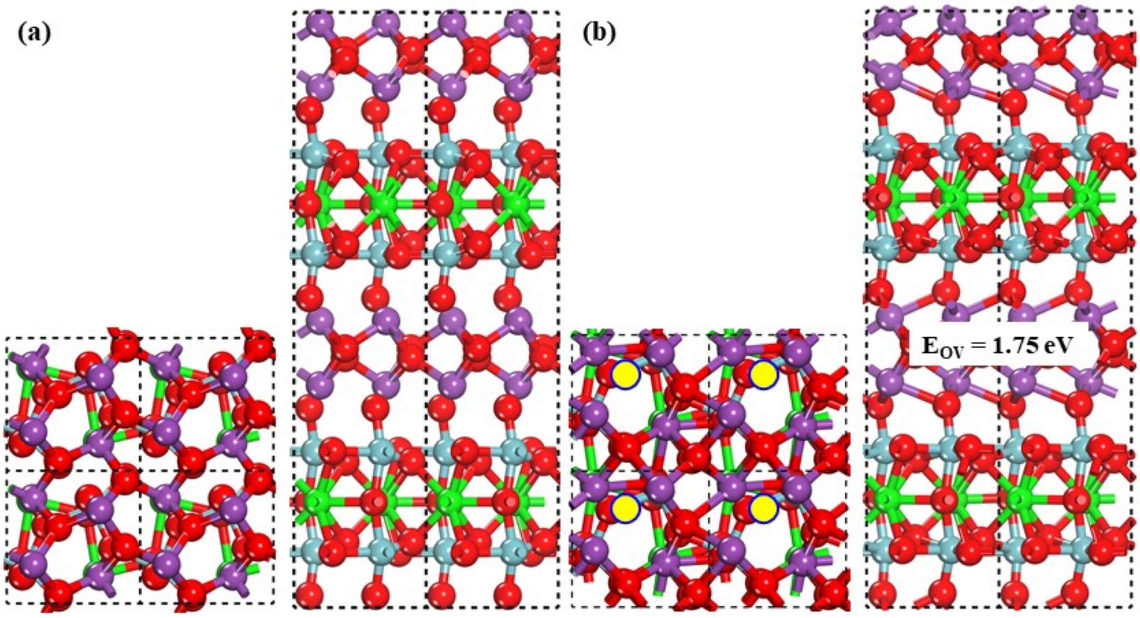

Figure S6. Calculated the structure and the vacancy formation energies of oxygen vacancies on the bulk of SBNO. (a) bulk of SBNO, (b) the oxygen vacancy of SBNO.

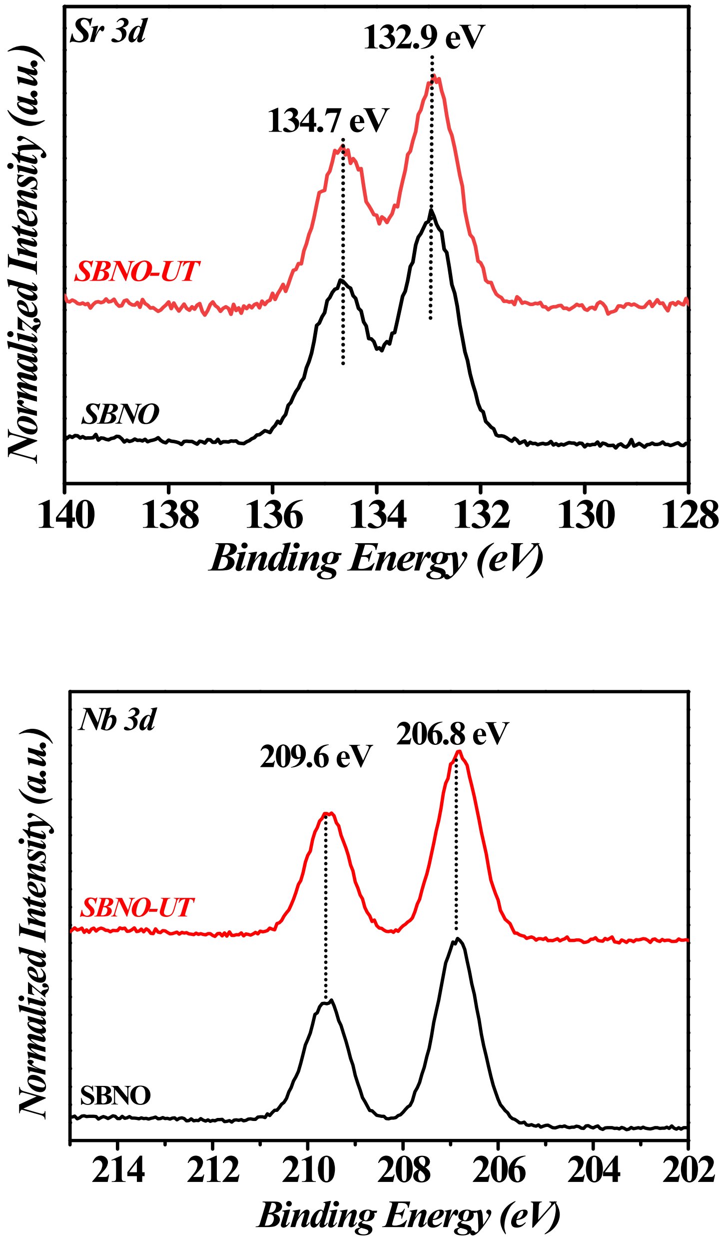

Figure S7. Comparative high resolution XPS spectra of Sr 3d and Nb 3d of SBNO and SBNO–UT, respectively.

Table S1. Comparison of the state-of-the-arts of reported photocatalysts for NO decomposition with light irradiation and high-temperatures.

Photocatalyst	Optimum conditions	Conversion (%)	Main products	Formed NO_2 (ppb)	S (%)	Ref.
TiO_2	0.019 g, 1040 ppb, 1 L/min NO in Air/N_2, 300 min	50.00 (in Air) 34.61 (in N_2)	NO_2, NO_3^-	490.1 and 581.2	0.0 and 50.0	[1]
Fe-doped TiO_2	0.019 g, 1040 ppb, 1 L/min NO in Air/N_2, 300 min	50.00 (in Air) 34.61 (in N_2)	N_2, O_2, NO_2, NO_3^-	490.1 and 581.2	0.0 and 50.0	[1]
Ag/TiO_{2-X}	500 ppb (in Air), 0.05 g, 420 nm, 21 min	45.0	N_2, O_2, NO_3^-	5.00	NG	[2]
g-C_3N_4	1500 ppb (in Ar), 0.1 g, Xe lamp 420 nm, 60 min	0.01	NO_2, NO_3^-	NG	0	[3]
C_v-g-C_3N_4	1500 ppb (in Ar), 0.1 g, Xe lamp 420 nm, 60 min	34.0	NO_2, N_2, NO_3^-	NG	66.0	[3]
TiO_2 with zeolites (Si/Al)	100 mg, Hg lamp (> 280 nm) 7.8 µmol NO	NG	N_2, O_2, N_2O	NG	88.0	[4]
Ti-HMS catalyst	100 mg, Hg lamp (> 280 nm) 25 ml/min, 7.8 µmol NO in He	NG	N_2, O_2, N_2O	NG	25.0	[5-6]
Cu^+/ZSM-5, Cu^+/Y-zeolite, Cu^+/SiO_2	Hg lamp (>280 nm) NO (2 ~20 Torr), 240 min	Cu^+/ZSM-5 the highest activity	N_2, O_2, N_2O	NG	NG	[7]
TiO_2 on ZSM-5	Hg lamp, 10 Torr NO	NG	N_2, O_2, N_2O	NG	NG	[8]

SBNO-UT nanosheets	120 mg, 13.5 ppm NO in Ar (800 ppb), 1.0 $L\cdot min^{-1}$, 180 min	19.72	N_2, NO_2, O_2, NO_3^-	12.24	0.004	This work
SBNO-UT nanosheets-Vo	120 mg, 13.5 ppm NO in Ar (800 ppb), 1.0 $L\cdot min^{-1}$, 180 min	47.63	N_2, O_2, NO_3^-	6.01	95.0	This work

*S is representing "Selectivity"; NG is "Not Given".

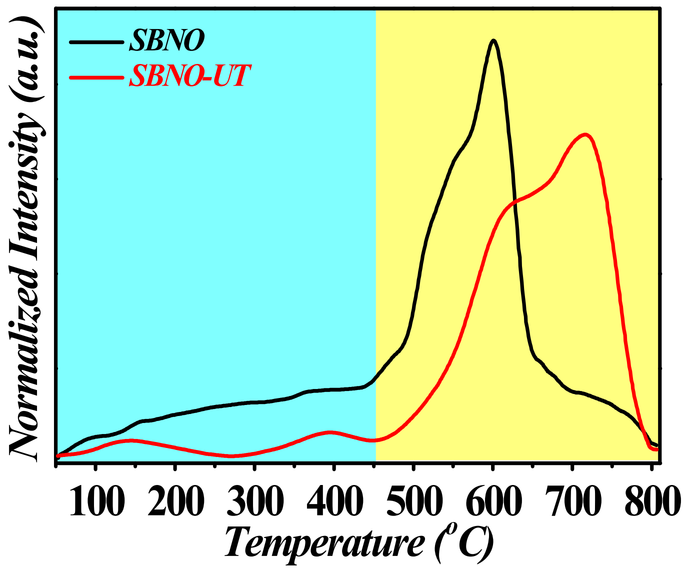

Figure S8. Comparative TPD−NO spectra of SBNO and SBNO−UT, respectively.

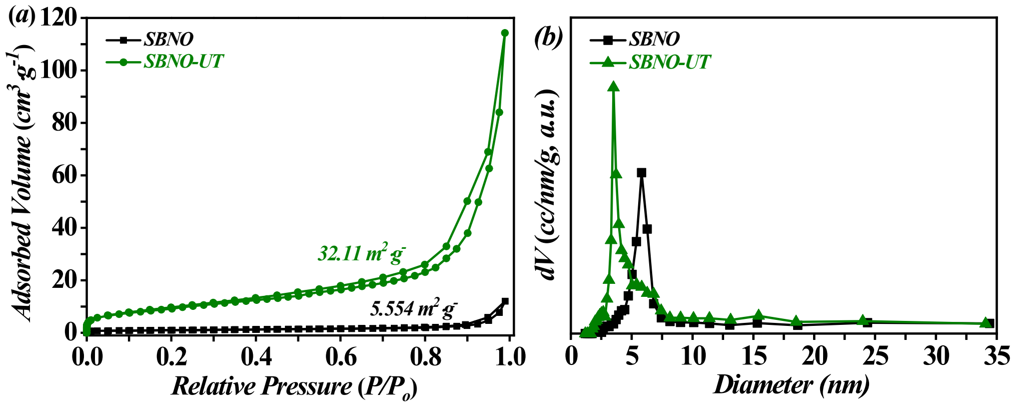

Figure S9. (a) Nitrogen adsorption-desorption isotherms, and (b) *pore size distribution* of SBNO and SBNO–UT, respectively.

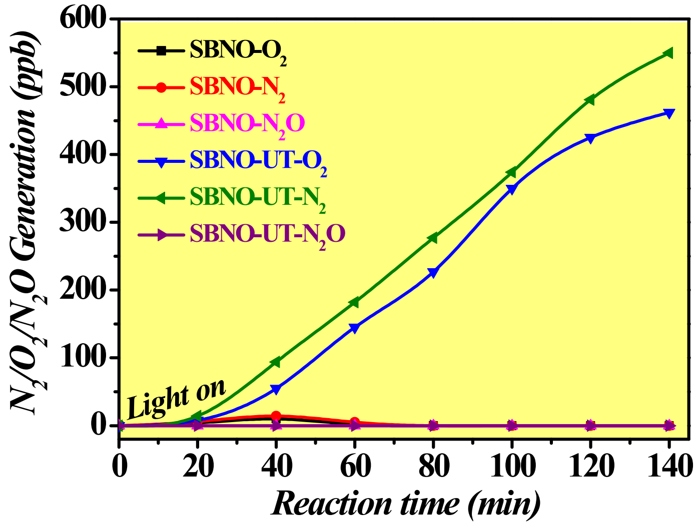

Figure S10. Formation of photocatalytic NO decomposition products with the assistance of SBNO and SBNO–UT, respectively.

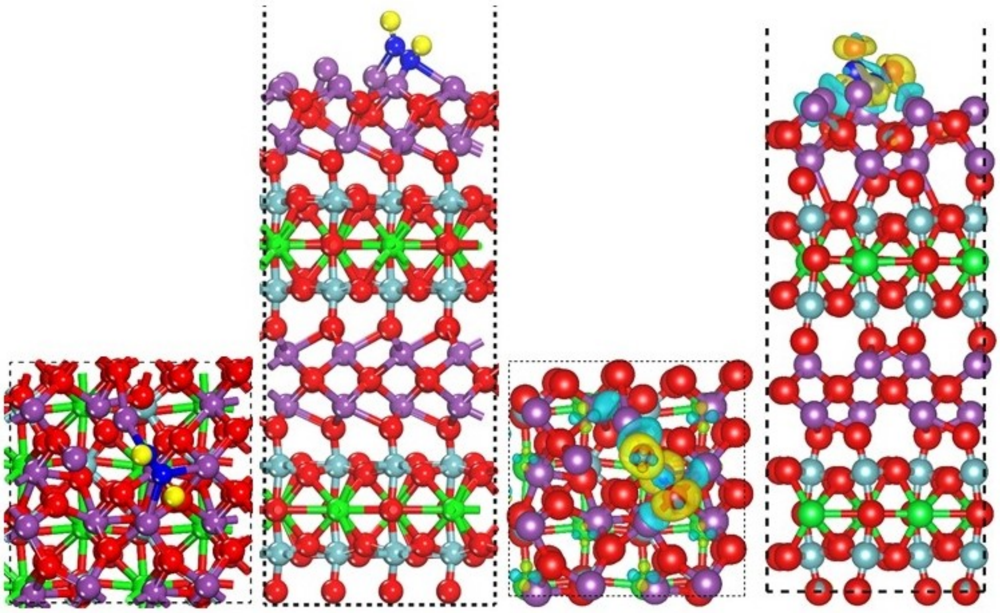

$E_{ads}(N_2O_2)$ = -1.03 eV

Figure S11. Calculated structures, spin-polarized charge densities and adsorption energies of two NO molecules adsorbed on SBNO–UT surface. Red: O atoms; green: Sr atoms; purple: Bi atoms; light blue: Nb atoms; Blue: N atoms, Yellow: O atoms in NO, respectively.

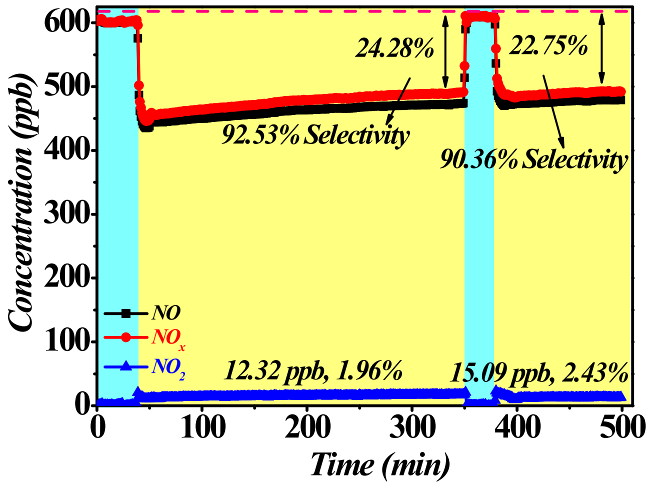

Figure S12. Long-term NO decomposition over defective SBNO–UT and light irradiation (NO in Ar).

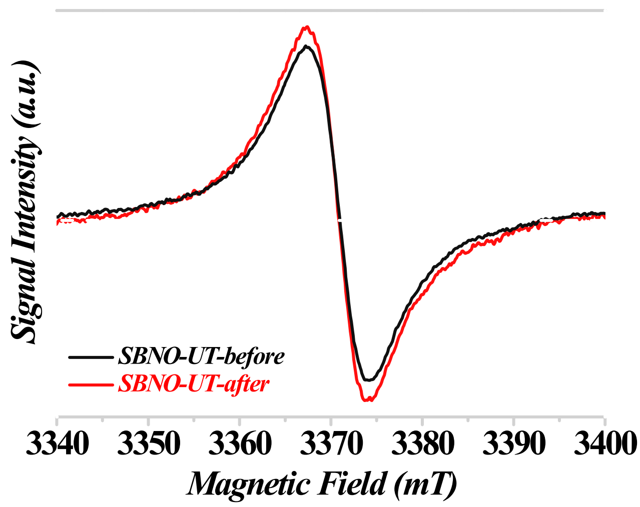

Figure S13. Comparative EPR spectra of SBNO–UT before and after the photocatalytic NO decomposition tests.

References:

(1) Q. P. Wu, R. V. D. Krol, Selective Photoreduction of Nitric Oxide to Nitrogen by Nanostructured TiO_2 Photocatalysts: Role of Oxygen Vacancies and Iron Dopant. *J. Am. Chem. Soc.,* 2012, ***134***, 9369−9375.

(2) Y. Y. Duan, M. Zhang, L. Wang, F. Wang, L. P. Yang, X. Y. Li, C. Y. Wang, Plasmonic Ag-TiO_{2-x} Nanocomposites for the Photocatalytic Removal of NO under Visible Light with High Selectivity: The Role of Oxygen Vacancies. *Appl. Catal. B-Environ.,* 2017, ***204,*** 67−77.

(3) G. H. Dong, D. L. Jacobs, L. Zang, C. Y. Wang, Carbon Vacancy Regulated Photoreduction of NO to N_2 over Ultrathin g-C_3N_4 Nanosheets. *Appl. Catal. B-Environ.,* 2017, ***218,*** 515−524.

(4) J. L. Zhang, Y. Hu, M. Matsuoka, M. Yamashita, M. Minagawa, H. Hidaka, M, Anpo. Relationship between the Local Structures of Titanium Oxide Photocatalysts and Their Reactivities in the Decomposition of NO. *J. Phys. Chem. B,* 2001, ***105*, **8395−8398.

(5) Y. Hua, S. Higashimoto, G. Martra, J. L. Zhang, M. Matsuoka, S. Coluccia, M. Anpo, Local Structures of Active Sites on Ti-MCM-41 and their Photocatalytic Reactivity for the Decomposition of NO. *Catal. Lett.,* 2003, ***90***, 3−4.

(6) J. L. Zhang, M. Minagawa, T. Ayusawa, S. Natarajan, H. Yamashita, M. Matsuoka, M. Anpo, In Situ Investigation of the Photocatalytic Decomposition of NO on the Ti-HMS under Flow and Closed Reaction Systems. *J. Phys. Chem. B,* 2000, ***104***, 11501−11505.

(7) M. Anpo, Approach to Photocatalysis at the Molecular Level Design of Photocatalysts, Detection of Intermediate Species, and Reaction Mechanisms. *Sol. Energy Mater. Sol. C.,* 1995, ***38,*** 221−238.

(8) S. C. Zhang, N. Fujii, Y. Nosaka, The Dispersion Effect of TiO Loaded over ZSM-5 Zeolite. *J. Mol. Catal. A,* 1998, ***129,*** 219−224.